SF 1075-SUR (3-2003) Supersedes (10-2002) issue

SANDIA REPORT

SANDNumber 2004-6421
Unlimited Release
Printed January 2005

Near Net Shape Forming Processes for Chemically Prepared Zinc Oxide Varistors

Nelson S. Bell, Steven J. Lockwood, James A. Voigt, and Bruce A. Tuttle

Prepared by
Sandia National Laboratories
Albuquerque, New Mexico 87185 and Livermore, California 94550

Sandia is a multiprogram laboratory operated by Sandia Corporation,
a Lockheed Martin Company, for the United States Department of Energy's
National Nuclear Security Administration under Contract DE-AC04-94AL85000.

Approved for public release; further dissemination unlimited.

Sandia National Laboratories

Issued by Sandia National Laboratories, operated for the United States Department of Energy by Sandia Corporation.

NOTICE: This report was prepared as an account of work sponsored by an agency of the United States Government. Neither the United States Government, nor any agency thereof, nor any of their employees, nor any of their contractors, subcontractors, or their employees, make any warranty, express or implied, or assume any legal liability or responsibility for the accuracy, completeness, or usefulness of any information, apparatus, product, or process disclosed, or represent that its use would not infringe privately owned rights. Reference herein to any specific commercial product, process, or service by trade name, trademark, manufacturer, or otherwise, does not necessarily constitute or imply its endorsement, recommendation, or favoring by the United States Government, any agency thereof, or any of their contractors or subcontractors. The views and opinions expressed herein do not necessarily state or reflect those of the United States Government, any agency thereof, or any of their contractors.

Printed in the United States of America. This report has been reproduced directly from the best available copy.

Available to DOE and DOE contractors from
U.S. Department of Energy
Office of Scientific and Technical Information
P.O. Box 62
Oak Ridge, TN 37831

Telephone: (865)576-8401
Facsimile: (865)576-5728
E-Mail: reports@adonis.osti.gov
Online ordering: http://www.doe.gov/bridge

Available to the public from
U.S. Department of Commerce
National Technical Information Service
5285 Port Royal Rd
Springfield, VA 22161

Telephone: (800)553-6847
Facsimile: (703)605-6900
E-Mail: orders@ntis.fedworld.gov
Online order: http://www.ntis.gov/help/ordermethods.asp?loc=7-4-0#online

SAND 2004-6421
Unlimited Release
Printed January 2005

Near Net Shape Forming Processes for Chemically Prepared Zinc Oxide Varistors

Nelson S. Bell and James A. Voigt
Chemical Synthesis and Nanomaterials Department

Steven J. Lockwood
Ceramic and Glass Department

Bruce A. Tuttle
Ceramic Materials

Sandia National Laboratories
P.O. Box 5800
Albuquerque, NM 87185-1411

Abstract

Chemically prepared zinc oxide powders are fabricated for the production of high aspect ratio varistor components. Colloidal processing in water was performed to reduce agglomerates to primary particles, form a high solids loading slurry, and prevent dopant migration. The milled and dispersed powder exhibited a viscoelastic to elastic behavioral transition at a volume loading of 43-46%. The origin of this transition was studied using acoustic spectroscopy, zeta potential measurements and oscillatory rheology. The phenomenon occurs due to a volume fraction solids dependent reduction in the zeta potential of the solid phase. It is postulated to result from divalent ion binding within the polyelectrolyte dispersant chain, and was mitigated using a polyethylene glycol plasticizing additive.

Chemically prepared zinc oxide powders were processed for the production of high aspect ratio varistor components. Near net shape casting methods including slip casting and agarose gelcasting were evaluated for effectiveness in achieving a uniform green microstructure achieving density values near the theoretical maximum during sintering. The structure of the green parts was examined by mercury porisimetry. Agarose gelcasting produced green parts with low solids loading values and did not achieve high fired density. Isopressing the agarose cast parts after drying raised the fired density to greater than 95%, but the parts exhibited catastrophic shorting during electrical testing. Slip casting produced high green density parts, which exhibited high fired density

values. The electrical characteristics of slip cast parts are comparable with dry pressed powder compacts.

Alternative methods for near net shape forming of ceramic dispersions were investigated for use with the chemically prepared ZnO material. Recommendations for further investigation to achieve a viable production process are presented.

Acknowledgements

The authors wish to acknowledge Stephen Zenker (formerly Department 14192, now Department 9621) for preparing the varistor powders used in these studies; Bonnie McKenzie for the SEM analysis, and Tom Headley for the TEM analysis.

Contents

Preface 9

Section 1: Milling and Dispersion of Powder *10*

Introduction 10

Experimental 11

Results 12

Discussion 23

Conclusions 27

Section 2: Near Net Shape Forming and Fired Electrical Properties *28*

Introduction 28

Experimental 29

Results 30

Discussion 36

Conclusions 38

Section 3: Alternative Processes *39*

Introduction 39

Other Procedures 40

References 42

Figures

FIGURE 1. ZINC IONS FROM CHEMICALLY PREPARED POWDERS AS A FUNCTION OF PH. CONCENTRATIONS ARE MEASURED FROM THE SUPERNATANT OF A 10 VOL% SUSPENSION AFTER AGITATION FOR 1 WEEK. LINES ARE PROVIDED TO GUIDE THE OBSERVER. 13
FIGURE 3A. MORPHOLOGY OF AS-RECEIVED POWDER (SEM MICROGRAPH). 15
FIGURE 3B. TEM MICROGRAPH OF COLLOIDALLY STABLE FINE PARTICLES AFTER 3 HOURS ATTRITION MILLING. 15
FIGURE 3C. SEM MICROGRAPH OF TOP LAYER OF SEDIMENT AFTER 3 HOURS ATTRITION MILLING. 16
FIGURE 3D. SEM MICROGRAPH OF MIDDLE LAYER OF SEDIMENT AFTER 3 HOURS ATTRITION MILLING. 16
FIGURE 3E. SEM MICROGRAPH OF THE BOTTOM LAYER OF SEDIMENT AFTER 3 HOURS ATTRITION MILLING. 17
FIGURE 4A. ZETA POTENTIAL VS. VOLUME FRACTION OF A SLURRY DISPERSED WITH 4 WT% DARVAN C (PMA) WITH RESPECT TO THE POWDER MASS. OPEN SYMBOLS ARE IN AQUEOUS SUSPENSION; HALFTONES ARE IN 10 WEIGHT % PEG400 (SLURRY PH = 9 FOR BOTH CONDITIONS). 18
FIGURE 4B. ZETA POTENTIAL AS BACKGROUND ELECTROLYTE IS INCREASED WITH KNO_3. SQUARES ARE FOR A 4.73 VOL% DISPERSED SUSPENSION IN PH 9 WATER, AND CIRCLES ARE FOR A 9.8 VOLUME % DISPERSED SUSPENSION IN 10 WEIGHT % PEG400. 19
FIGURE 5. ZETA POTENTIAL OF AS SYNTHESIZED POWDER AND POST MILLING AT PH 11 AND PH 12. 20
FIGURE 6. INTRINSIC VISCOSITY OF CPV POWDER DISPERSED WITH 4 WT% DARVAN C IN PH 9 WATER (SQUARES) AND IN A FLUID MIXTURE OF 10% PEG400-90% PH 9 WATER. LINES ARE PLOTS OF THE MODIFIED KRIEGER-DOUGHTERY EQUATION WITH PARAMETERS $\phi M = 0.582$, $[\eta] = 5.3$ AND $\phi M = 0.63$, $[\eta] = 4.84$. 21
FIGURE 7. STRESS SWEEP VS. ϕ FOR THE CPV POWDER MILLED AND DISPERSED WITH 4 WT% DARVAN C IN WATER. A. ELASTIC MODULUS VS. STRESS. B. LOSS MODULUS VS. STRESS. 22
FIGURE 8. VISCOSITY OF A 32 VOLUME % CPV SLURRY AT CONSTANT SHEAR RATE DURING HEATING. THE FLUID PHASE CONTAINS 10 WEIGHT % PEG400 PLASTICIZER AND 1 WT% AGAROSE GELATOR. THE TEST SHEAR RATE IS 200 SEC^{-1}. 31
FIGURE 9. VISCOSITY VS. SHEAR RATE AT 90 °C FOR THREE TEST FLUIDS. A. 1 WT% AGAROSE, 10WT% PEG400 SOLUTION AND NO CPV ZINC OXIDE POWDER. B. 32 VOL% CPV DISPERSED SUSPENSION WITH 10% PEG400 IN FLUID PHASE. C. 32 VOL% CPV DISPERSED SUSPENSION WITH 10% PEG400; 1% AGAROSE IN FLUID PHASE. 32
FIGURE 10. ELASTIC MODULUS COMPARISONS DURING COOLING FOR THE AGAROSE GELATION PROCESS MEASURED AT A SHEAR STRESS OF 0.1 PA AND A FREQUENCY OF 1 HZ. A. 1 WT% AGAROSE, 10WT% PEG400 SOLUTION AND NO CPV ZINC OXIDE POWDER. B. 32 VOL% CPV DISPERSED SUSPENSION WITH 10% PEG400, NO AGAROSE IN FLUID PHASE. C. 32 VOL% CPV DISPERSED SUSPENSION WITH 10% PEG400; 1% AGAROSE IN FLUID PHASE. 32
FIGURE 11. SOLUBILITY COMPARISIONS FOR ZINC, ALUMINUM, AND BISMUTH IONS VS. PH FOR ROOM TEMPERATURE AGING AND AGING AT 90 °C. 33
FIGURE 12. SINTERED MICROSTRUCTURE (SEM) OF (A) DRY ISOPRESSED, (B) SLIP CAST, (C) AGAROSE GEL CAST, AND (D) AGAROSE GEL CAST PARTS FOLLOWED BY ISOPRESSING AT 103.4 MPA. 34
FIGURE 13. CURRENT DENSITY-FIELD CHARACTERISTICS OF ISOPRESSED AND SLIP CAST TEST SAMPLES. 35

Tables

TABLE 1. COMPOSITION OF ZINC OXIDE POWDER..... 11
TABLE 2. SURFACE AREA OF MILLED POWDER AS A FUNCTION OF MILLING TIME 14
TABLE 3. MILLING RESULTS AT ELEVATED PH 20
TABLE 4. MEASUREMENTS OF FABRICATED PARTS..... 30

Preface

The chemically prepared zinc oxide varistor powder is agglomerated, and can be broken down into nanosized and submicron-sized particles using attrition milling, which is functionally complete in one hour. This step is also used for the dispersion of the powder to form a colloidal slurry. Processing in this report has been performed in aqueous solution, and the maximum solids content in a low viscosity slurry occurs near 45 volume%. The stability of the material and the dopants to chemical leaching in water is critical for this processing step. Heating in water increases the solubility of the material and destabilizes the suspension. This leads to increased viscosity, poor castability and low density final parts. An unfired density of ~ 50 volume % solids was shown to form fired parts exceeding 95 % theoretical density.

Parts formed at room temperature by slip casting achieved the near theoretical packing density predicted by geometrical modeling of packed spheres. These parts also performed well in electrical testing. The casting time is very long (i.e. 10-14 days) and some parts showed drying flaws that limit the height of the sample produced.

The future processing of these materials in nonaqueous solvents would eliminate the destabilization resulting from solubility of the material. Routes for successful part production include the use of injection molding, a system with thermally controlled particle stability or casting using thermally sensitive binders (such as polymethyl methacrylate polymers) to control gelation.

Near Net Shape Forming Processes for Chemically Prepared Zinc Oxide Varistors

Section 1: Milling and Dispersion of Powder

Introduction

Colloidal processing of ceramic materials has led to the development of several novel forming methods for casting bulk ceramic preforms (1). These processes can be superior to conventional forming methods when structural uniformity is a key issue and in situations where loss of material from post-sintering machining and finishing processes has a significant cost impact. Often of equal importance to product quality is the negative affect that machining-induced flaws can have on performance. For example, in varistor elements, material defects or flaws (such as machining cracks or pores) can severely impact electrical performance (2). Inhomogeneities can concentrate the pulse current and initiate the high voltage breakdown of the varistor. The purpose of the work presented here was to investigate the application of colloidal processing-based forming methods to prepare high field ZnO varistor components.

The varistor powder used in this study was prepared using an aqueous precipitation process developed at Sandia National Laboratories (3-6). One of the challenges of developing colloidal forming processes using these powders is that their primary particles are below 200 nm in size. This small size makes them highly sinterable, but complicates slurry processing. Bergstrom et al. have shown for very fine particle size powders that there is a significant effect on densification dependent upon the particle interactions and formation of a homogeneous green microstructure (7). This implies that achieving a maximum solids loading in the slurry, and optimizing the formation method effects on green structure will dictate the success of part production.

Rheological characterization is commonly used to determine the maximum solids loading using the Krieger-Doughtery expression (1).

$$\eta = \eta_s \left(1 - \frac{\phi}{\phi_{\max}}\right)^{-[\eta]\phi_{\max}} \qquad (1)$$

In this expression, ϕ is the true volume fraction with a maximum at ϕ_{max}, η is the slurry viscosity, η_s is the solvent viscosity and $[\eta]$ is the intrinsic viscosity, which relates to the effect on the relative viscosity of non-interacting particles in very dilute suspensions. It represents a particle shape factor beginning at 2.5 for spheres and increasing with shape anisotropy. Cube-shaped particles have a value of 4 for example (8). A plot of the high shear rate viscosity against volume fraction can be fit with this equation to estimate the volume fraction of close packed particles.

In this study, the processing parameters related to the formation of a colloidally stable, high solids loading suspension of the chemically prepared varistor material were investigated. The solubility of the material versus pH, and the effectiveness of a polyelectrolyte dispersant were examined as solids loading increased. The rheological characteristics of the suspension were studied and fitted with a modified Krieger-

Doughtery equation to estimate the maximum packing fraction that can be achieved in the suspension. The use of processing aids such as a plasticizer was also tested.

Experimental

The composition of the chemically prepared zinc oxide is as given in Table I. These powders are produced by a three step process, the first of which is the aqueous coprecipitation of the chloride salts of Zn, Mn, Co, and Al, followed by a Bi doping step and finally a Na doping step (3). Powder density was measured by helium pycnometry[1] to be 5.58 g/cm^3.

Table 1. Composition of Zinc Oxide Powder.

Zinc Oxide	98.94 mole %
CoO	0.25 mole %
MnO	0.25 mole %
Bi_2O_3	0.56 mole %
Al	135 ppm
Na	300 ppm

The chemical stability of the powder was evaluated by leaching studies using ammonium hydroxide to adjust pH. Five volume % concentrations of powder were aged for one week under shaking, and the supernatant was characterized for each dopant by Inductively Coupled Plasma Mass Spectroscopy (ICP) analysis[2]. The uncertainty of these measurements is ±10%.

Attrition milling with three mm yttria stabilized zirconia media was used to achieve a mill solid loading of 40 volume %. Ammonium polymethacrylate[3] (PMA) was used as dispersant at 4 % to the powder dry weight. The particle size of the dispersed and milled powder was studied using dilute suspensions (< 0.01 wt%) by a Coulter LS230 light scattering device[4]. Surface area was measured using the BET method[5]. Zeta potential was measured after the addition of PMA and the milling operation using a DT 1200 acoustic spectrometer[6]. A concentrated suspension at pH 9 was measured for acoustic attenuation and speed of sound, conductivity and colloid vibration impedance, and the data used to determine particle size distribution and zeta potential. The suspension was successively diluted with deionized water pre-adjusted to pH 9 with ammonium hydroxide. The solid loading for each dilution was determined by weight loss. A 4.73 volume % suspension was titrated at pH 9 using 1.0M KNO_3 solution to measure zeta potential as conductivity is increased. Similar measurements were performed on a dispersion containing 10 weight % PEG400 in the fluid phase, and a suspension at 9.8 volume % CPV powder was titrated at pH 9 with KNO_3 to compare zeta potential with monovalent salt concentration.

---

[1] VP Penta-Pyncnometer, Quantachrome Corp., 1900 Corporate Dr., Boynton Beach, FL 33426.
[2] Elan 6000 ICP/MS, Perkin- Elmer, 710 Bridgeport Ave., Shelton, CT 06484-4794.
[3] Darvan C, R.T. Vanderbilt Company, Inc., 30 Winfield St., Norwalk, CT 06855.
[4] Coulter LS230, Coulter Corp., P.O. Box 169015, Miami, FL 33116-9015.
[5] ASAP 2010, Micromeritics, One Micromeritics Dr., Norcross, GA, 30093-1877.
[6] DT1200 Acoustic Spectrometer, Dispersion Technology, 3 Hillside Ave., Mount Kisco, NY 10549.

A second milling study was initiated using basic solutions of ammonia with the chemically processed ZnO powder, and ball milling for three days. The suspensions were measured for particle size using the acoustic spectrometer, and then titrated with nitric acid (1.0 M) to measure the effect of the basic milling on the isoelectric point.

Rheology of the suspension was measured as a function of volume fraction using a Haake RS 300 Rheometer with a 60 mm diameter titanium 1° cone and flat plate geometry[7]. The evaporation of solvent was prevented by use of a polycarbonate solvent trap and paraffin oil. Shear rates were increased from a static condition to the maximum rotation speed, held for one minute, and decreased to the initial speed. Tests were made of the powder dispersed using PMA and following the addition of poly(ethylene glycol) 400 (PEG400) at 10% by mass of the fluid mass as a plasticizing agent.

Results

The chemical stability of the powder in an aqueous environment is important as leaching of the dopant elements to the solvent could cause changes in the electrical performance of the varistors. Results of powder leaching at various pH's are shown in Figure 1. The surface chemistry of the synthesized powder should resemble that of bismuth oxide, as the bismuth is added after the precipitation and calcination of the doped zinc oxide powder. However, milling operations used to reduce particle size will allow the zinc and dopant elements to leach as well. Clearly, the minimum in solubility of all elements is pH 9.1. Maintaining this pH during slurry processing is important to prevent the segregation of dopants in the microstructure, and avoid particle agglomeration via specific adsorption of ionic species to the particles, which reduces electrostatic stabilization.

[7] Haake Instruments, 53 W. Century Rd., Paramus, NJ 07652.

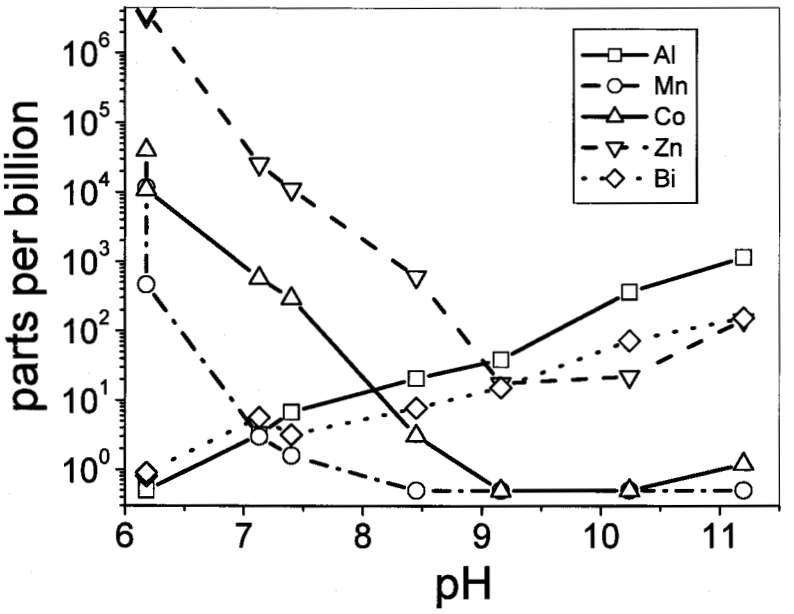

Figure 1. Zinc ions from chemically prepared powders as a function of pH. Concentrations are measured from the supernatant of a 10 vol% suspension after agitation for 1 week. Lines are provided to guide the observer.

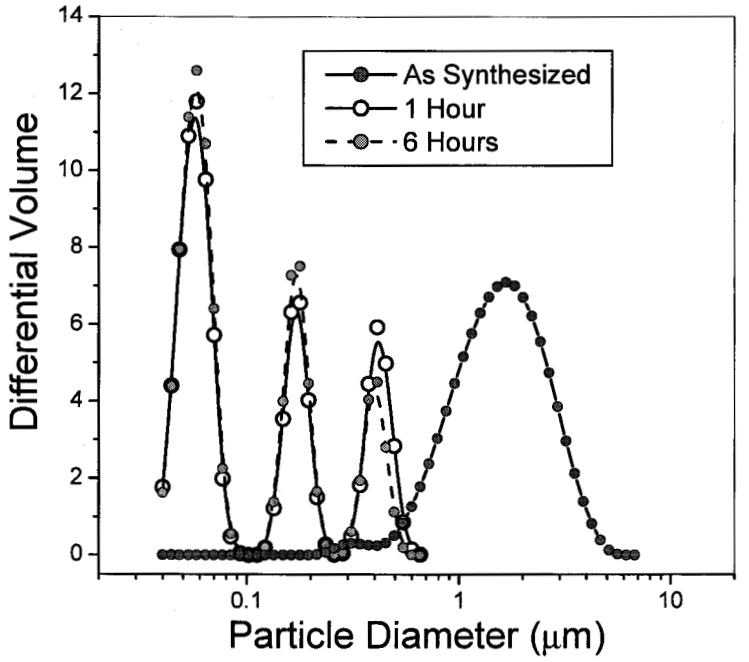

Figure 2. Particle size distributions showing the effect of the attrition process on the initial powder distribution, after one hour of attrition milling, and following six hours of attrition milling. Lines are provided to guide the observer.

The particle size distributions of the initial powder and after various milling times are presented in Figure 2. The distribution of particle sizes shows that fragmentation of the initial particle agglomerates occurs and produces three distinct size fraction peaks. Long milling times did not reduce these agglomerates. Table 2 presents the surface area data measured using N_2 adsorption. An increase in surface area appears complete within one hour of attrition milling.

Table 2. Surface Area of Milled Powder as a Function of Milling Time

Milling Time	Specific Surface Area (m^2/g)
Initial	8.66 ± 0.03
15 minutes	11.12 ± 0.04
30 minutes	11.17 ± 0.04
45 minutes	11.19 ± 0.05
60 minutes	11.15 ± 0.04

Figure 3 shows the morphology of the synthesized powder, and the morphology of particles separated by sedimentation over the course of a month. The initial particles are aggregated to each other, where the agglomerates retain the morphology of the oxalate crystalline structure formed during precipitation. The apparent particle size is ultrafine and in the range of 50 nm. However, the agglomerates are "hard" with strong necks to nearest neighbors. Maximizing the solids fraction in the slurry requires milling to the primary or near primary particle size.

Figure 4A shows the zeta potential measured on these particles after adding 4 weight % PMA at pH 9 and the corresponding conductivity of each sample as a function of volume fraction solids in aqueous solution and in a solution of 10 weight % PEG400. The PMA generates a negative zeta potential and adds a steric stabilization component from the adsorbed polymer chains (9,10). The magnitude of the zeta potential at high solids concentration is relatively low, and the magnitude increases as solvent is added. In Figure 4B, the zeta potential of a 4.73 volume % suspension was measured during titration of KNO_3 electrolyte solution to characterize the screening of the PMA dispersed powder against salt addition. The zeta potential decreases in magnitude with added monovalent salt, but not as rapidly as found for the samples in Figure 4A. The zeta potential decreases with volume fraction more rapidly than can be attributed to the effects of electrolyte concentration alone. The addition of PEG400 inhibits the decline in zeta potential as solids loading is increased, but follows the same qualitiative trend with conductance.

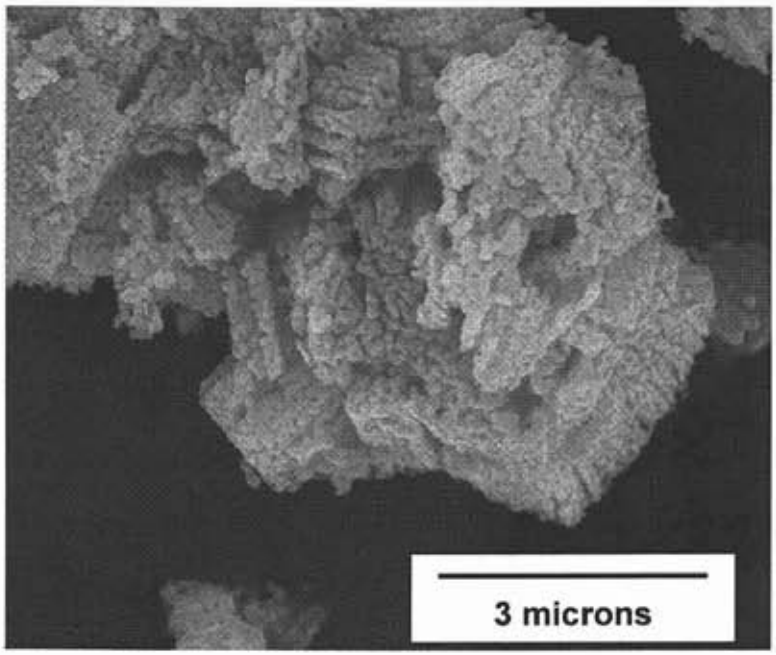

Figure 3A. Morphology of as-received powder (SEM micrograph).

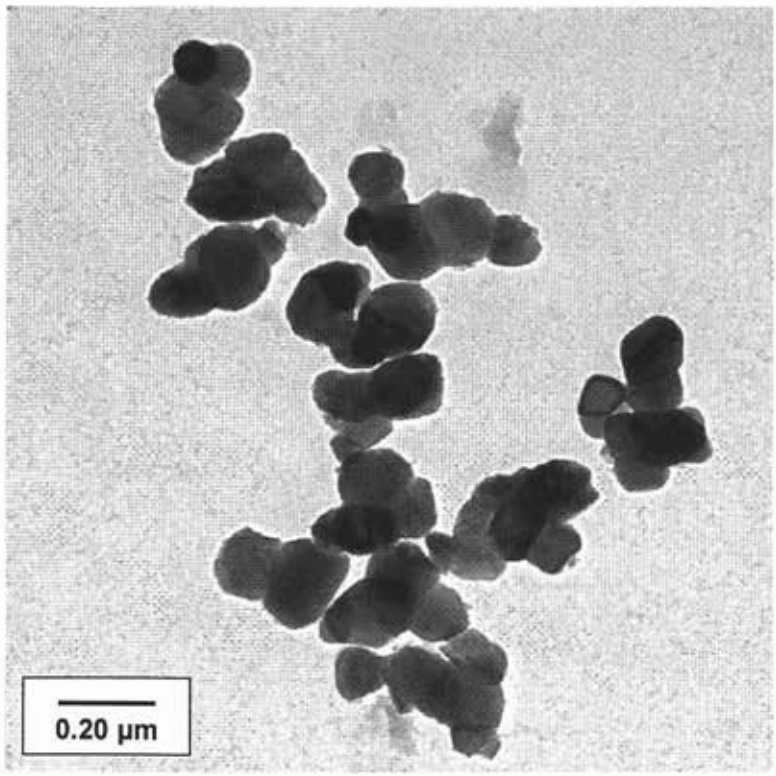

Figure 3B. TEM micrograph of colloidally stable fine particles after 3 hours attrition milling.

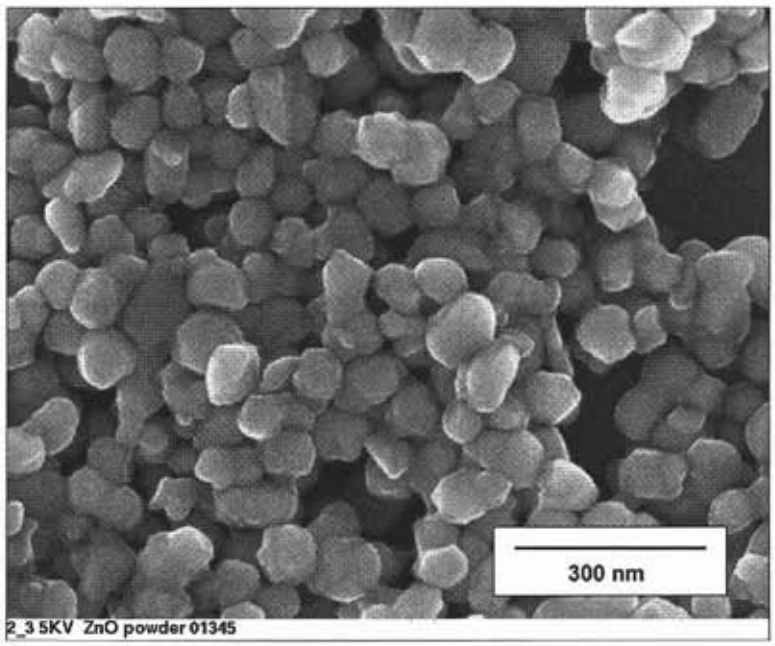

Figure 3C. SEM micrograph of top layer of sediment after 3 hours attrition milling.

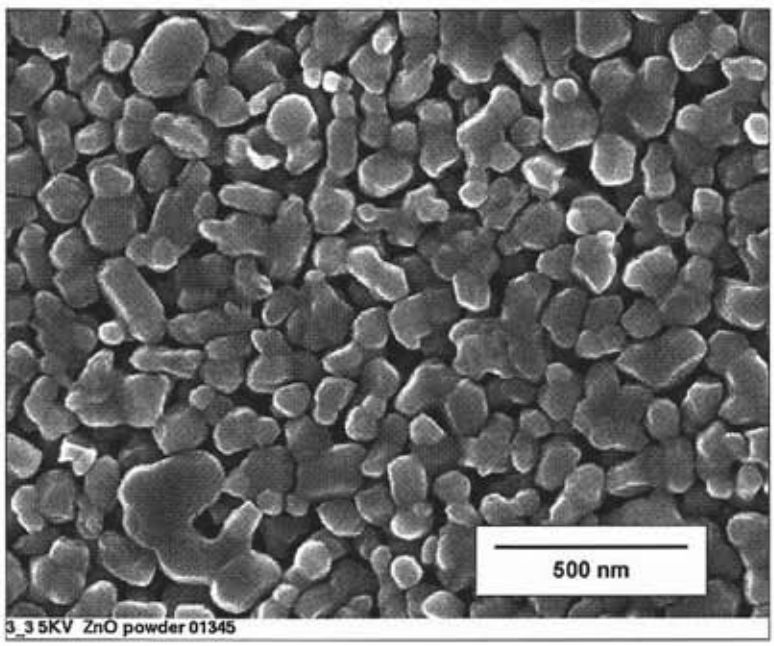

Figure 3D. SEM micrograph of middle layer of sediment after 3 hours attrition milling.

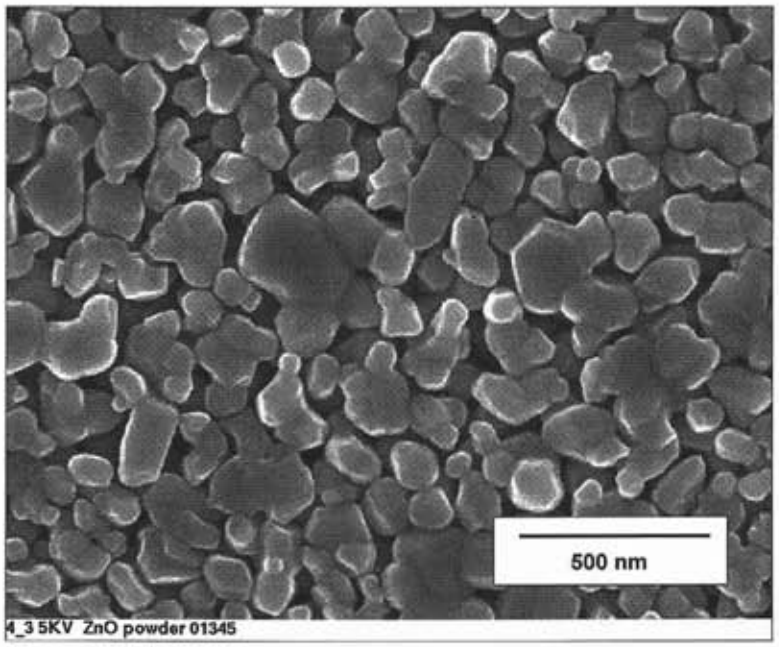

Figure 3E. SEM micrograph of the bottom layer of sediment after 3 hours attrition milling.

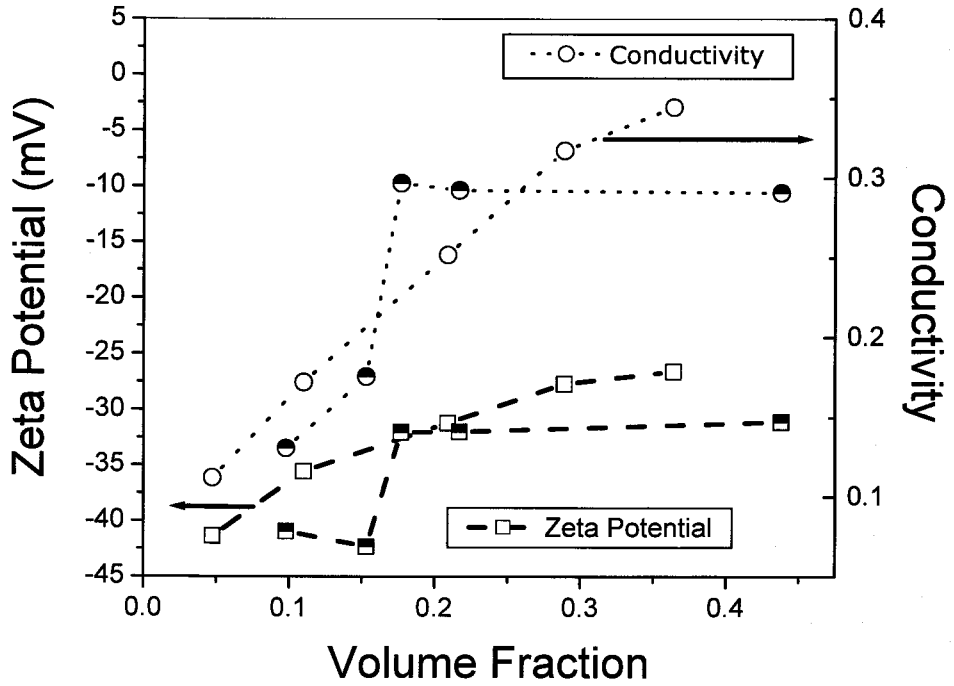

Figure 4A. Zeta potential vs. volume fraction of a slurry dispersed with 4 wt% Darvan C (PMA) with respect to the powder mass. Open symbols are in aqueous suspension; halftones are in 10 weight % PEG400 (slurry pH = 9 for both conditions).

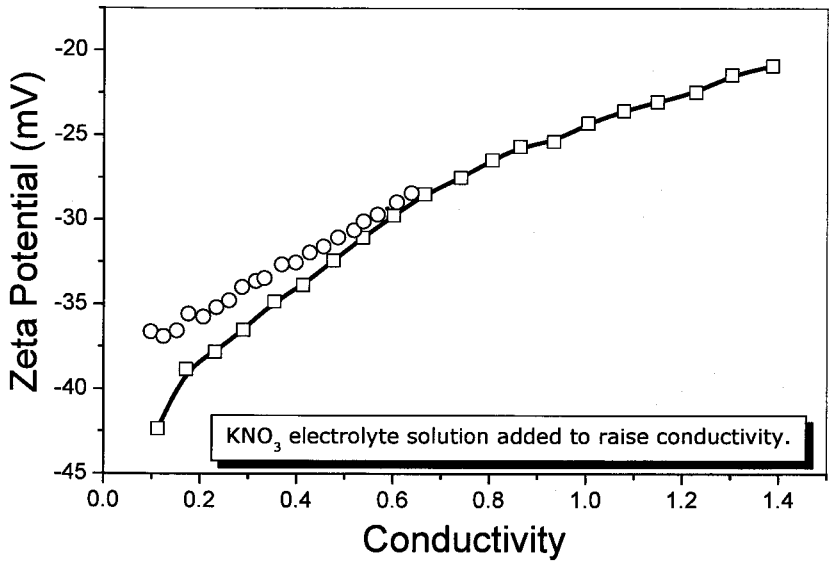

Figure 4B. Zeta potential as background electrolyte is increased with KNO_3. Squares are for a 4.73 vol% dispersed suspension in pH 9 water, and circles are for a 9.8 volume % dispersed suspension in 10 weight % PEG400.

The second milling study using basic ammonia solutions generated bimodal particle size distributions as given in Table 3. From the data, milling at increasing pH was effective in lowering the particle size of the powder, and milling at pH 12 was more effective at reducing large agglomerates and giving a lower mean size.

Table 3. Milling Results at Elevated pH

Solution pH	Mode 1	Mode 2	Mean	Standard Dev	% Large
Mill @ pH 11	73 nm	732 mn	503 nm	0.24	0.55
Mill @ pH 12	75 nm	400 nm	268 nm	0.27	0.45

The isoelectric points were also determined by titration with nitric acid, and are presented in Figure 5. The as synthesized powder has a clear isoelectric point at pH 8.6, and significant magnitudes in zeta potential as pH varies from the isoelectric point. In both milling conditions at basic pH, the isoelectric point has shifted to extremely high pH values. The decrease in zeta potential for the powder milled at pH 11 and tested near pH 6 is an artifact of increased ionic strength. The powder solubility becomes so great at pH 7 and lower, that the ionic strength in solution collapses electrostatic stabilization.

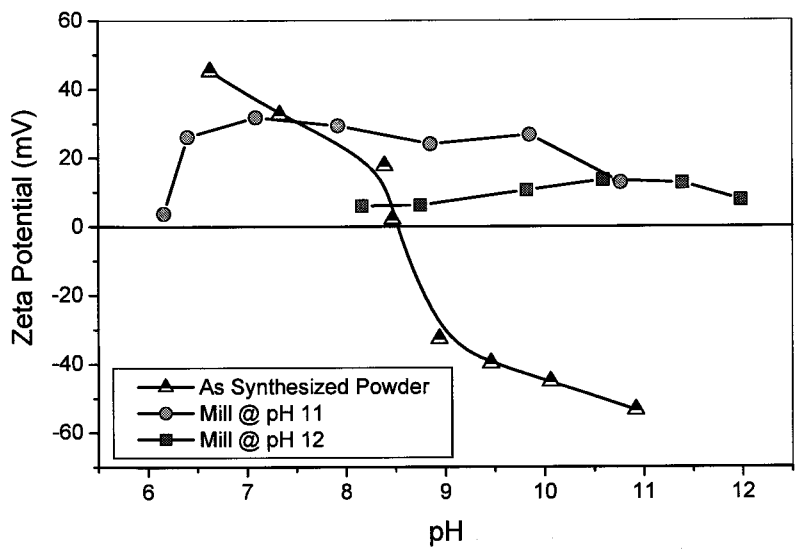

Figure 5. Zeta potential of as synthesized powder and post milling at pH 11 and pH 12.

Rheological characterization was performed to determine the role of volume fraction on viscosity in the suspension and colloidal stability. Figure 6 shows the power law relationship of the relative viscosity (η/η_s) versus volume fraction at a high shear rate of 750 sec^{-1}. Fits to the modified Krieger-Doughtery equation (equation 1) for the effect of volume fraction on viscosity produce equation parameters of $\phi m = 0.582$ and $[\eta] = 5.3$

for the PMA dispersed powder in water and $\phi m = 0.63$ and $[\eta] = 4.84$ for the PMA dispersed powder with 10 weight % PEG400 added to the liquid phase.

Figure 7 shows an oscillatory stress sweep at 1 Hz for increasing volume fractions of the PMA dispersed slurry. As solids content is increased, the elastic modulus (G′) becomes greater in magnitude than the loss modulus (G″) and constant over the shear stress sweep. The solid volume fraction that causes the elastic transition is not exactly identified, but lies between 38 and 41 volume %. These graphs show the development of a particle structure as volume fraction is increased. At the highest measured solids loading, elastic behavior is dominant over the entire measured range. It was not possible to characterize the exact volume fraction where a contacting particle network is formed, but estimates from our experience suggest that it ranges from 43-46 vol% dependent on the powder lot.

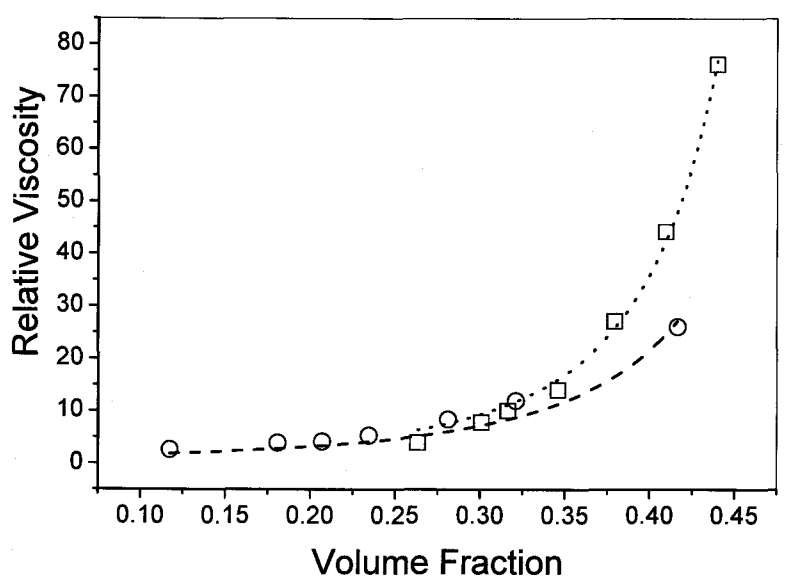

Figure 6. Intrinsic viscosity of CPV powder dispersed with 4 wt% Darvan C in pH 9 water (squares) and in a fluid mixture of 10% PEG400-90% pH 9 water. Lines are plots of the modified Krieger-Doughtery equation with parameters $\phi_m = 0.582$, $[\eta] = 5.3$ and $\phi_m = 0.63$, $[\eta] = 4.84$.

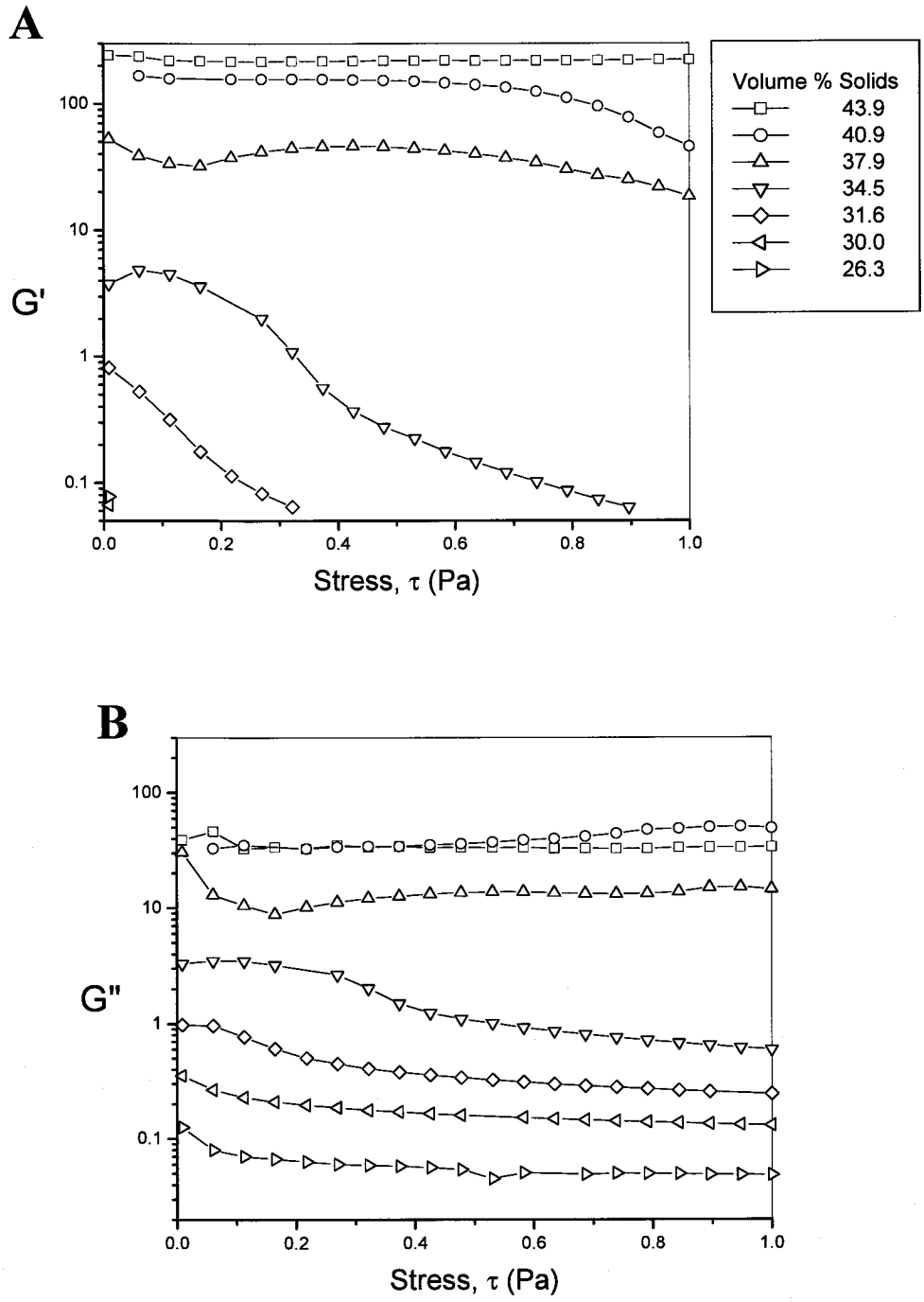

Figure 7. Stress sweep vs. ϕ for the CPV powder milled and dispersed with 4 wt% Darvan C in water. A. Elastic modulus vs. stress. B. Loss Modulus vs. stress.

Discussion

The solubility of dopants in the synthesized powder was evaluated first to determine the stability of the material in water. Leaching should be minimized to prevent dopant segregation. The leaching or dissolution of components mimics the expected solubility of the metal hydroxides given by hydrolysis reactions of the dopants (11). As shown in Figure 1and using Baes and Mesmer's speciation compilation (11), below pH values of 9, the mononuclear Zn^{2+} species was the primary solution component, and above pH 11, the $Zn(OH)_4^{2-}$ became the soluble species. Aluminum dissolves as $Al(OH)_4^-$ above pH 6. Manganese in the 2+ state has a number of hydrolysis products that decrease in solubility as pH increases. The mononuclear species precipitate above pH 9 –10 depending on solution concentration. Cobalt is stable in water in the 2+ state, and the mononuclear species continually decreases in concentration to pH 10 where the hydroxide is stable. Bismuth becomes highly soluble below pH 8 due to the formation of polynuclear species ($Bi_9OH_{22}^{5+}$, $Bi_9OH_{21}^{6+}$), but between pH 8 and 12, the hydroxide phase is dominant. The slight rise in Bi^{3+} observed in these tests relates to the formation of $Bi(OH)_4^-$. With the exception of bismuth species, the low concentrations measured in the solution suggest that polynuclear species do not play a large role in leaching. The lowest concentration of dopants was found to be at pH 9.1. Maintaining this value of pH should enhance material stability.

The attrition milling process used in slurry preparation was functionally complete in one hour. Table 2 shows the specific surface area of the powder at intervals of this first hour. Significant increases in surface area are not indicated by the data, though particle size distributions shown in Figure 2 clearly show the breakdown of the aggregates. Maximizing a size reduction process requires consideration of particle stability, energy input and milling time. Since attrition milling inputs a large amount of energy into grinding, it is not likely that further operations will reduce the particle size.

It is clear that the porous aggregates are fracturing into distinct populations, which are stable against further milling. A dilute particle suspension was allowed to sediment, and particles were sampled as a function of stability and sedimentation time to examine the milled particle morphology. Scanning electron micrographs of sedimentation fractions of the milled powder cannot distinguish distinct particle size fractions shown in Figure 3. Distinct separation of particle sizes as seen in the particle size distribution data was not possible. There is a difference in morphology of the most stable particles (smallest size) and the rapidly sedimented particle fraction (largest size). The highly stable particles are roughly equiaxed and approximately 50 nm in diameter. Their small size promotes their stability to gravimetric sedimentation, and the dispersant prevents particle agglomeration. The largest particles are sintered aggregates of submicron-sized particles with distinct grain boundaries between the aggregates rather than the porous structure of the synthesized aggregates. The approximate size of the aggregates is 400 nm, and their arrangement is non-equiaxed. The individual grains within the large size aggregates are approximately 100-200 nm in size. Based on these observations, we propose that the as synthesized aggregates are constructed as a surface layer of nanosized particles with a core of more strongly aggregated submicron-sized grains. The intermediate grains between the core and exterior are larger than the nanosized fraction, and lie in the range of 100-200 nm. The milling process fractures the necks between

crystallites to separate the nanosized and intermediate populations, but does not provide enough energy to fracture the core aggregates.

The milling tests performed under basic conditions were an attempt to apply the principles of chemically aided milling. The Bismuth oxide is theorized to be concentrated in the interior of the synthesized powder aggregates. As Bismuth ions become soluble under basic conditions, milling at pH 11 and 12 is expected to attack those regions that bind the large aggregates together. From the particle size data in Table 3, it appears that our theory is correct. The highest pH condition reduced the particle size of the large aggregates more than milling at pH 11. This has undoubtedly affected the powder surface chemistry, as characterized in Figure 5. It is unknown if the preferential leaching of Bismuth will affect the processing of the powder, and in the interest of maintaining the dopant ratios to provide the target varistor characteristics, further studies were not investigated.

Particle dispersion was performed as a component of attrition milling. Ammonium polymethacrylate (PMA) was used to increase the zeta potential of the particles under this pH constraint, and provide a steric component to repulsion due to the adsorbed polymer chains. The amount of dispersant necessary to form a high solids loading slurry is relatively large. Concentrations near 4 weight % to powder weight were necessary to form a fluid slurry of high solids content.

Often, colloidal stability is characterized by the value of zeta potential. For dispersions of nanopowders, the counterion concentration generated by the surface area and the amount of dispersant added generates significant salt levels. Conductivity was used to characterize the electrolyte level in the PMA dispersed suspensions. Figure 5A plots the measured particle zeta potential as a function of the volume fraction of solids, and conductivity of the suspensions is also plotted for reference. Figure 5B shows the zeta potential at a constant solids loading of 4.73 volume% as the conductivity is increased by the addition of KNO_3 electrolyte solution. By comparison of the two graphs, it is clear that increasing solids content by itself does not raise the salt level beyond 0.35. At low volume fraction, this does not reduce the zeta potential by a significant amount, but for the samples at high volume solids the zeta potential is significantly reduced. Clearly, the reduction in zeta potential is not caused by increased monovalent electrolyte concentration alone.

The decreasing strength of the zeta potential directly impacts the flow properties of the suspensions. The effects of solids loading are shown by the rheology characterization measurements, given in Figure 6. The figure shows the slurry viscosity at 750 sec^{-1} and a least squares fit of the modified Krieger-Doughtery equation. The parameters of this equation are commonly used to characterize the maximum packing fraction of the slurry in the linear viscosity region, and a particle shape parameter. For the PMA dispersed suspension, $\phi m = 0.582$, and $[\eta] = 5.3$. The shape factor of the equation is reasonable in comparison with the morphologies shown in Figure 3 as the larger particle fractions are slightly non-equiaxed and show some grain boundaries, but does not forbid the presence some small aggregates or particle doublets.

Although the modeling of the shear rate data suggests that a maximum solids loading approaching 58% solids can be achieved, our experience with this powder showed that a hard packed body is formed at volume fractions solids of near 43-46%. In Figure 7, the oscillatory characteristics of the PMA dispersed suspension under a shear

stress sweep at 1 Hz are presented. As volume fraction is increased, the elastic modulus G′ becomes increasingly strong and constant over the stress range investigated, and the viscoelastic component G″ is stronger at low volume fraction, but weaker above a transition near 38 volume %. Clearly, the PMA dispersed particles are developing elastic characteristics at unexpectedly low volume fractions. As zeta potential values are decreasing with volume fraction, the elastic properties are likely developed as a result of weak attraction forces between particles or the development of a weak interparticle network similar to a particle gel.

The unusual phenomenon in this system is the reduction in zeta potential strength as solids loading is increased. The zeta potential of the dispersed material is controlled by the adsorbed polyelectrolyte, and the interactions of the solution components with the polyelectrolyte will dictate its effectiveness as a dispersant. The tests in Figure 5B showed that counterions do screen the electrostatic charge of the dispersant layer to lower the measured zeta potential, but the effect is much stronger as volume fraction is increased than can be explained by the conductivity of the solution. Solids fraction effects were previously considered to reduce zeta potential by Johnson et al. (12), who applied an empirical correction. However, the instrument used in our studies uses a complete theory that requires no volume fraction correction and therefore the zeta potential reduction is real (13-15). An additional factor in this material is the large number of dopants, which exhibit varying degrees of solubility and valence in solution.

The interaction between polyelectrolyte adsorbed layers and plurivalent counterions affect the adsorbed amount and conformation of the layer in addition to having stronger electrostatic screening effects (16,17). Abraham et al. have shown that force curves between anionic polyelectrolytes are sensitive to the addition of divalent cations (18). All divalent cations screen the forces between the polyelectrolyte chains, and specific adsorption of the cations to the solid surface can eliminate negative charged sites on the substrate and promote higher adsorbed amounts. From the speciation chemistry investigated for the particle solubility vs. pH, the only positively charged species in this system at pH 9.1 are Zn^{2+} ions, and the dispersion pH is very close to the onset of very high zinc solubility. The relatively high concentration of dispersant necessary for slurry formation suggests that zinc dissolution is affecting the polyelectrolyte adsorption. Abraham et al. found that the incorporation of Ca^{2+} ions with poly (acrylic acid) adsorbed brushes created a complex profile of long-range stabilization, an attractive short-range regime at intermediate separation, and a short-range repulsive interaction at close separations. The attractive intermediate regime was attributed to divalent ion induced bridging between layers in their study. We have performed all processing as close to the minimum in solubility as possible, but there is no guarantee that some dissolution does not occur during attrition milling. In fact, increased solubility of zinc ions during milling would explain the relatively high concentration of dispersant found necessary to disperse this powder.

Ammonium polymethacrylate is known to form chemical complexes with Zn^{2+}, and the binding energy of Zn^{2+} is stronger than that of Ca^{2+}. (16). The adsorption of divalent cations can be represented according to the apparent equilibrium constant for the complexation reaction, with the assumption that the bound Zn^{2+} ions form a dimeric complex.

$$k_{app} = \frac{[Zn^{2+}]_{bound}}{[Zn^{2+}][-COO^-]^2}$$

(2)

If the zinc concentration is raised in the solution, the complexation reaction will be promoted to achieve chemical equilibrium. If $[Zn^{2+}]$ is decreased in the solution, bound Zn^{2+} in the dispersant layer would be likewise released. This process would affect the particle zeta potential in accord with our observations. As solvent is removed to concentrate the solids loading, any dissolved zinc ions in solution become more concentrated and reduce the value of the measured zeta potential. At some critical complex concentration, the value of the particle zeta potential would be insufficient for dispersion of the particles and a particle gel would form. This gel might involve binding between dispersant layers on adjacent particles as well.

Although this hypothesis appears to incorporate all our observations, we cannot claim that it is the definitive phenomenon causing the instability of the particles in this dispersion. A more focused study is required to answer this question completely.

Addition of PEG400 Plasticizer

The PMA dispersed suspension with 10 weight % PEG400 has modified Kreiger-Doughtery equation parameters of $\phi m = 0.63$ and $[\eta] = 4.84$. Figure 5 shows that the zeta potential is more resistant to increases in volume fraction of solids when PEG400 is present in the solution phase. The effect of monovalent electrolyte seems to converge in the suspensions tested. In Figure 6, the data indicates that the addition of PEG400 reduces the high shear viscosity of the suspensions, and raises the maximum solids loading. Oscillatory measurements were also conducted for these suspensions, but the elastic components were largely below detection limits for the instrument below the highest volume fraction. These equation parameters suggest that the particle morphologies are more equiaxed after its addition, but the values remain similar to the observed particle morphologies. The lowering of the shape factor and increase of the maximum packing fraction suggests that PEG400 is increasing particle stability and inhibiting the formation of flocculated particles at high solids loading.

The action of PEG400 to improve the stability of the particles at high solids loading suggests that it interacts within the dispersant layer to prevent the hypothesis of divalent ion binding. Solutions of polyethylene oxide and polymethacrylate have been extensively studied for their hydrogen bonding interactions, and it is accepted that the polymers do have an interaction leading to precipitation, although this is only seen at very low degrees of ionization of the polymethacrylate (19). In the case of polymer layers, the argument of low degree of ionization appears modified (20-22). Netz showed that the dielectric constant of the interface affects the dissociation reaction of an adsorbed polyelectrolyte (22). Podhajecka et al. found that the degree of polyelectrolyte dissociation near the interface does not correspond to the bulk pH, and the polyethylene oxide segregated to the non-polar interface to form an interpolymer complex that resists bulk conditions very strongly (20). Based on these studies, it is plausible that PEG400 acts as a very low molecular weight polyethylene oxide polymer and intercalates within the inner layers of the polymethacrylate dispersant to provide a stronger steric repulsion between particles.

Therefore, the argument is strong that multivalent ion complexes forming within the dispersant layers of the particles explain the behavior seen in this powder. As solids loading increases, ion binding is proposed to reduce the zeta potential. As colloidal stability decreases, the flocculated structures are formed which raise viscosity and prevent the attainment of high solids loading. The addition of PEG400 inhibits the formation of this attractive force through intercalation within the dispersant layer and increased repulsion. This delays the formation of flocculated structures and allows for the achievement of higher solids loadings with fluid response.

Conclusions

A chemically prepared, doped zinc oxide powder was characterized and processed for near net shape forming methods of colloidal processing. The minimum in component solubility was found in aqueous solution at pH 9.1. The initial material was aggregated, and attrition milling with ammonium polymethacrylate was largely successful in breaking down the aggregates into primary particles. The primary particles exhibit a trimodal distribution, in which the largest fraction is composed of the remaining hard aggregates. Suspensions of these materials exhibited a viscoelastic to elastic behavioral transition at relatively low volume concentrations between the range of 38 – 41 volume % solids. The mechanism for this transition involved a reduction in the zeta potential of the dispersed particles, and is proposed to relate to chemical complexation of zinc ions within the dispersant layers. As solids loading increases, zinc ions are concentrated in the solution, which promotes the binding interaction and reduces zeta potential. The addition of polyethylene oxide 400 to the solution phase greatly reduced the elastic component of the particle suspensions for the evaluated solids loading. The reduction of the attractive interaction between particles is proposed to relate to intercalation of the polyethylene oxide within the ammonium polymethacrylate layers to inhibit ion binding between particles. This allows for the attainment of higher solids loading in suspension.

Section 2: Near Net Shape Forming and Fired Electrical Properties

Introduction

The fabrication of varistor components that meet target electrical breakdown characteristics require processing materials into geometries that minimize flaws, inhomogeneities and compositional gradients. Powder processing of mixed oxides to form varistors have traditionally mixed the desired component oxides in the target ratio, and sintered the material at temperatures that promote the diffusion of all components to form a homogeneous microstructure. The high temperatures needed can promote the formation of large grain sizes (1-5 micron) and thereby impact the electrical characteristics. A doped zinc oxide material has been developed at Sandia National Laboratories in which the desired additives are incorporated in the material during fabrication, and in which the average primary particle size is < 200 nm (3-6). This allows for the formation of uniform microstructures at low temperatures, and with average grain sizes of half a micron. A near net shape forming technique is desired which provides a uniform green body microstructure and fired properties within the desired material processing range.

The use of traditional dry pressing techniques is not suitable for this application because the high aspect ratio of the parts creates difficulty in forming a uniform green body. Die filling and the powder/die wall friction during compaction make it difficult to prepare compacts of uniform density. Near net shape casting methods such as slip casting and gelcasting can significantly reduce inhomogeneity in parts. However, slip casting can show particle size segregation in the green part and exhibits sensitivity to rheology (23). Additionally, the casting rate of slip casting relates to the microstructure of the cake and has a parabolic relationship to casting time. Flocculation in a slip leads to the formation of larger voids in the cast part and a lower green density. High density occurs when a high solids loading slurry with low viscosity is used for the casting, but requires long casting times.

Gelcasting of suspensions of ceramic materials reduces microstructural inhomogeneity in cast parts and eliminates material waste associated with machining pressed parts into complex shapes (24) The use of agarose as a gelling agent for ceramic processing utilizes the variable solubility of agarose polymer in water to add green strength to a finished part (25-27). Agarose is soluble in water above 90°C, but has a large hysteresis before gelation at ~37°C (28). In the production of uniform parts, the formation of a homogeneous green structure is critical for the formation of uniform bodies. The powder under investigation has a primary particle size less than 200 nm in diameter, and the presence of large voids in the green structure would significantly impact the densification and electrical properties of the final varistor components.

Both slipcasting and gelcasting techniques were evaluated for their applicability to varistor component production. Colloidal processing effects on dispersed slurry characteristics, green body microstructure, densification behavior and varistor electrical performance are presented.

Experimental

The solubility of the powder was measured at 90 °C by holding a dilute suspension of powder at elevated temperature for one week, and evaluating the ionic concentration using Inductively Coupled Plasma Mass Spectroscopy (ICP) analysis[8]. The uncertainty of these measurements is ±10%. The adjustment of pH was performed using nitric acid and ammonium hydroxide solutions.

All tests of the slurry used powder dispersed with ammonium polymethacrylate[9] (PMA) and following the addition of poly(ethylene glycol) 400 (PEG400) at 10 weight% of the fluid phase as a plasticizing agent. Rheological measurements of the agarose solutions and PMA dispersed zinc oxide slurry were measured using a Haake RS 300 Rheometer with a 40 mm cup and bob geometry[10]. Tests were performed at constant shear rate upon heating of the suspension, as a function of shear rate at 90 °C, and in oscillation at 0.1 Pa applied stress and a frequency of 1 Hz as the samples were cooled from 90 to 20 °C. The evaporation of solvent was prevented by use of a polycarbonate solvent trap and a cover layer of low viscosity paraffin oil.

Slurry formulations were tailored for each production method. A tall cylindrical mold was fixed to a porous plaster of Paris substrate, and slip cast parts were formed under ambient conditions. Agarose injection molding was utilized at 1.0 weight percent agarose to water concentrations. The dry agarose powder was added to the 40 Vol % slurry and mixed on a Specs mill with 1 cm diameter Yttria stabilized ZrO_2 milling media to homogenize the slurry. The slurry was placed in a sealed casting chamber and heated to 90°C under mechanical agitation. After 30 minutes at 90°C, the temperature was decreased to 70°C and a vacuum was applied to remove entrapped air bubbles. An overpressure of 138 kPa was then applied, and parts were cast into molds. The molds were refrigerated for 30 minutes before demolding. Samples dried at ambient conditions. After drying, some agarose samples were isopressed at 103.4 MPa to test further densification. Mercury porosimetry was performed to characterize the pore structure[11].

Organic additive burnout of the compacts was performed by heating at 0.5 °C/minute to 500 °C for a hold time of four hours. Sintering took place under a ZnO powder bed in an enclosed crucible. The schedule for sintering heated the samples at 1 °C/minute to 732 °C with a hold time of 16 hours, followed by normal cooling to room temperature. The finished parts were characterized for density by the Archimedes method, and polished specimens were prepared for microstructural and electrical characterization.

Varistor elements for electrical testing that were approximately 1 cm in diameter and 1 mm thick were sliced from fired varistor ceramics using a diamond wafering saw. Varistor surfaces were then prepared for electroding using 600 grit SiC abrasive. Gold electrodes of 200 nm thickness and 5mm to 8 mm diameter were sputter deposited onto the varistor surface. DC electrical test measurements were performed at nominal current densities of 10^{-6}, 10^{-5}, 10^{-4}, 10^{-3} and 5×10^{-3} A/cm^2. A Keithley Model 619

---

[8] Elan 6000 ICP/MS, Perkin- Elmer, 710 Bridgeport Ave., Shelton, CT 06484-4794.
[9] Darvan C, R.T. Vanderbilt Company, Inc., 30 Winfield St., Norwalk, CT 06855.
[10] Haake Instruments, 53 W. Century Rd., Paramus, NJ 07652.
[11] AutoPore Mercury porosimeter IV 9500 V1.05, Micromeritics Co., One Micromeritics Dr., Norcross, GA 30093.

electrometer/multimeter (Cleveland, OH) and a Gamma High Voltage Research DC power supply (Model RR3-50P) were used in conjunction with a Hewlett Packard HP3478A multimeter (Colorado Springs, CO) to measure the DC current – voltage characteristics. Pulse measurements were made at nominal current densities of 2.5 A/cm^2, 5 A/cm^2 and 10 A/cm^2. A 30 μsec pulse width was used for these measurements. A Velonex pulse generator model 660P (Santa Clara, CA) and a SONY/Tektronix 390AD programmable digitizer (Tokyo, Japan) were used for the pulse measurements.

Results

A number of forming techniques were tested to see the effect on consolidated microstructure. Uniaxial pressing was used to determine a baseline green density for the powder as synthesized. Slip casting of the milled and dispersed powder gives a measurement of the effectiveness of colloidal formation routes. Agarose gelcasting was evaluated for use as a production method, and isopressing of agarose cast parts was used in an attempt to improve green and sintered density. Table 4 gives the average green density of each of these methods. Mercury porosimetry was used to characterize the pore size distribution of each of the green parts formed by these methods. The green body porosity information as well as the sintered density is also given in Table 4.

Table 4. Measurements of Fabricated Parts

Method	Green Part % Theoretical Density	Average Sintered Pore Size (nm) 4V/A	Average Sintered Theoretical Density (g/cm^3)
Slip Casting	61.7 ± 2.7	36.6	97.5 ± 3.0
Isopressing As Received powder	46.6 ± 0.8	58.4 ± 0.2	92.0 ± 0.4
Agarose Gelcasting (1wt%)	49.9 ± 0.9	50.5 ± 6.5	87.6 ± 7.2
Agarose Gelcasting with Isopressing	52.5 ± 1.6	45.1 ± 6.8	95.1 ± 2.1

Rheological characterization was performed on solutions containing 10 weight% PEG400 and 1 weight% agarose, as well as a 32 vol% dispersion of the chemically prepared doped zinc oxide powder with 10 weight% PEG400 in the fluid phase as a plasticizing agent (called the CPV slurry hereafter). Figure 8 shows the viscosity of the CPV slurry with 1 weight% agarose in the fluid phase during initial heating at a shear rate of 200 sec^{-1}. There is a clear rise in viscosity beginning near 45 °C and peaking at 80 °C before dropping at 95 °C. Figure 9 shows the decreasing shear rate curve for a solution of agarose (1 weight%) in 10 weight% PEG400 aqueous solution, the CPV slurry, and the CPV slurry with 1 weight % agarose at 90 °C where the agarose is expected to be completely dissolved. Figure 10 presents the elastic modulus of the agarose/PEG400 solution, the CPV slurry, and the CPV slurry with 1 weight% agarose as temperature is decreased from 90 to 20 °C. The applied stress is 0.1 Pa and the frequency is 1 Hz in

these measurements, which was found to be in the linear elastic gel regime from initial testing.

The solubility of the chemically prepared powder at 90 °C was measured and compared with data from room temperature aging in Figure 11. Under the slurry pH of 9.1, the concentrations of zinc and bismuth ions were found to increase by approximately an order of magnitude.

The microstructure of the specimens is presented in Figure 12, and isolated porosity is obvious in the samples. The fired grain size was near the target value of 0.5 microns, and there is little evidence of abnormal grain growth. The current-voltage (I-V) response of the samples is illustrated in Figure 13, indicating similar varistor behavior of the slip cast and isopressed samples. Agarose gelcast parts exhibited catastrophic shorting; data was not available for these samples.

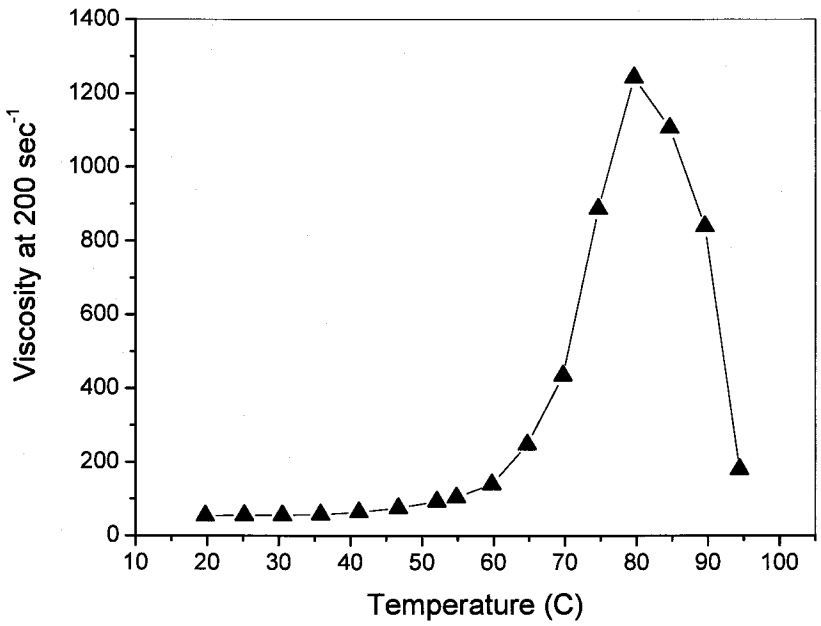

Figure 8. Viscosity of a 32 volume % CPV slurry at constant shear rate during heating. The fluid phase contains 10 weight % PEG400 plasticizer and 1 wt% agarose gelator. The test shear rate is 200 sec^{-1}.

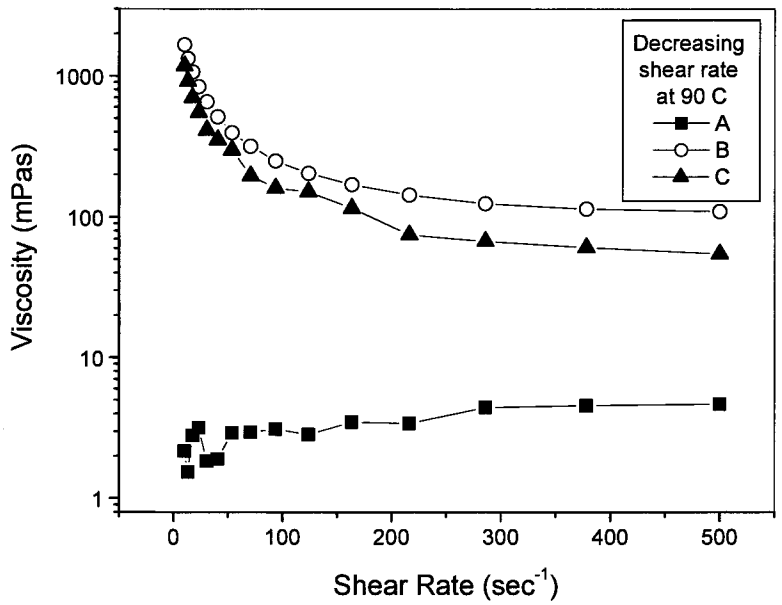

Figure 9. Viscosity vs. shear rate at 90 °C for three test fluids. A. 1 wt% agarose, 10wt% PEG400 Solution and no CPV zinc oxide powder. B. 32 vol% CPV dispersed suspension with 10% PEG400 in fluid phase. C. 32 vol% CPV dispersed suspension with 10% PEG400; 1% agarose in fluid phase.

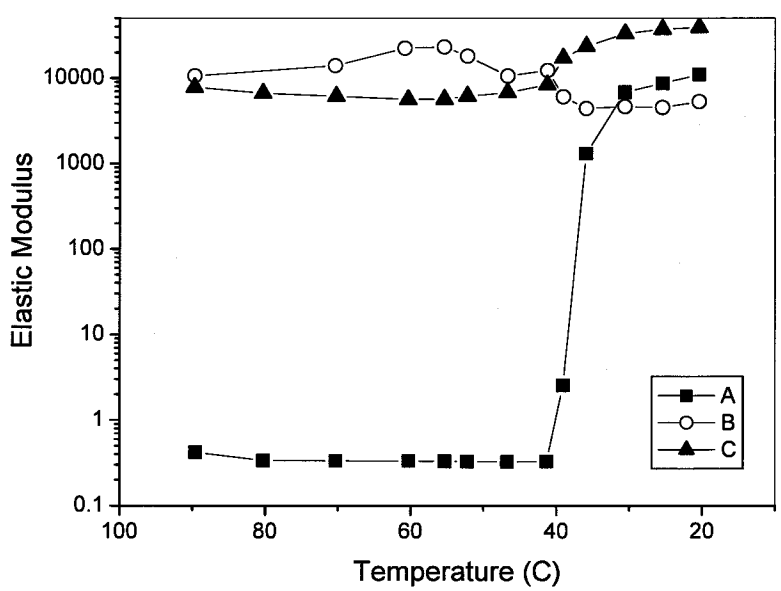

Figure 10. Elastic modulus comparisons during cooling for the agarose gelation process measured at a shear stress of 0.1 Pa and a frequency of 1 Hz. A. 1 wt% agarose, 10wt% PEG400 Solution and no CPV zinc oxide powder. B. 32 vol% CPV dispersed suspension with 10% PEG400, no agarose in fluid phase. C. 32 vol% CPV dispersed suspension with 10% PEG400; 1% agarose in fluid phase.

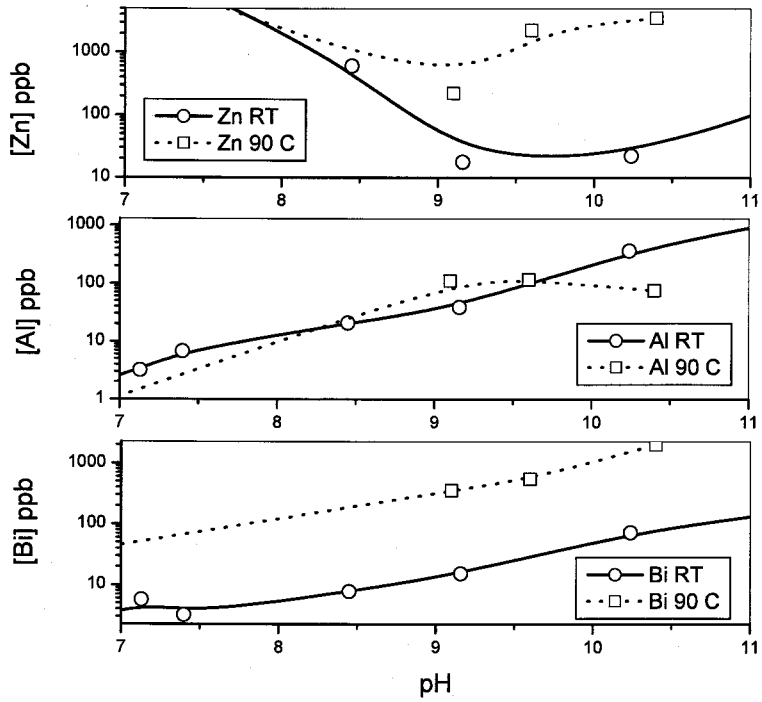

Figure 11. Solubility comparisions for zinc, aluminum, and bismuth ions vs. pH for room temperature aging and aging at 90 °C.

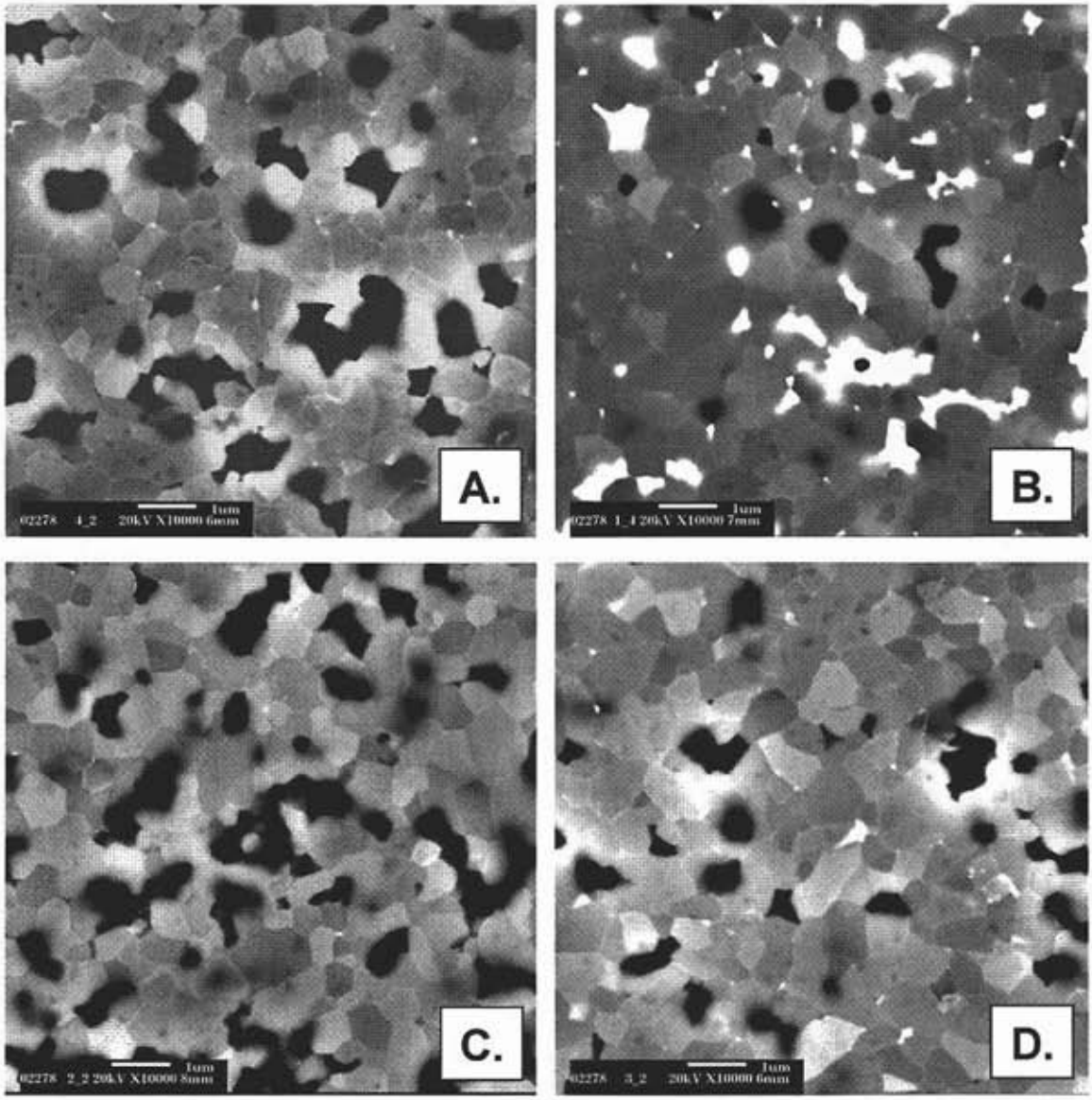

Figure 12. Sintered microstructure (SEM) of (A) dry isopressed, (B) slip cast, (C) agarose gel cast, and (D) agarose gel cast parts followed by isopressing at 103.4 Mpa.

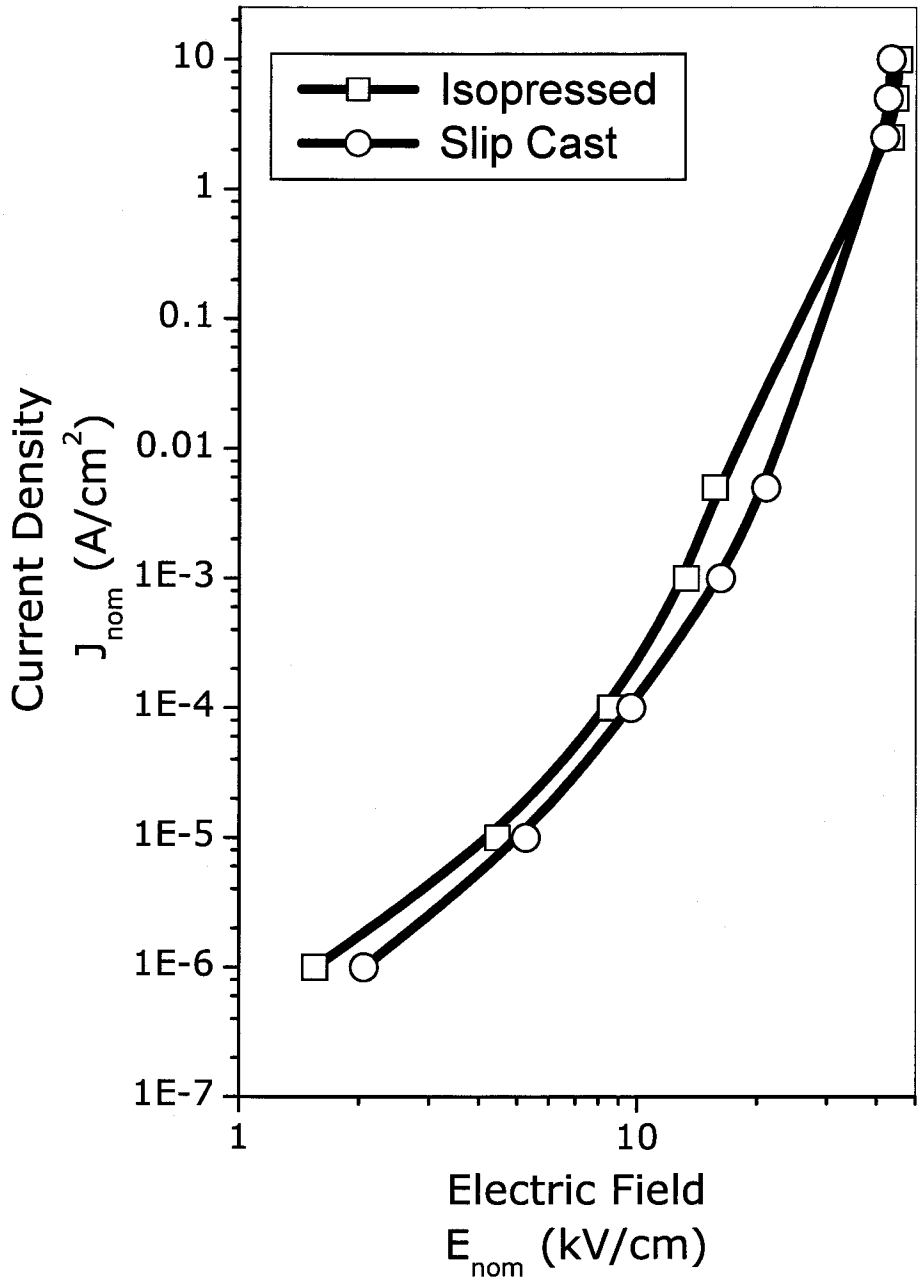

Figure 13. Current density-field characteristics of isopressed and slip cast test samples.

Discussion

The rheological measurements tested in this study were performed to evaluate the interactions between particles during the heating and gelation process of the agarose polymer. In the study of the dispersion of these powders, it was proposed that the dissolution of the zinc cations could cause ion binding between the dispersant layers and prevent the attainment of high solids loading slurries (see Section 1). Figure 8 shows increases in viscosity of the slurry which begins at ~45 °C. This is much lower than that expected to result from the dissolution of the agarose polymer. Figure 9 shows that the viscosity of the CPV slurry is much higher than the agarose/PEG400 solution, and the addition of agarose actually seems to lower the viscosity of the CPV slurry slightly. The values determined here are a factor of 4-5x higher than that noted for a suspension at room temperature. This is a clear indication that some colloidal instability is occurring during the heating period and at elevated temperature. Figure 10 shows the progress of the gelation process during cooling. The use of PEG400 at 10 weight% was not found to prevent the gelation of the agarose solution, as it begins to increase elastic modulus at 37 °C as described in the literature. Our measurements with purely aqueous solutions show that the G′ values in the gelled state are also comparable. The CPV slurry has a very high value of G′ that decreases slightly but not completely as temperature is lowered. Colloidal stability is not spontaneously retrieved on cooling the slurry. For the addition of agarose to the CPV slurry, the elastic modulus is lower but comparable above the agarose gel point, and increases similarly to the agarose solution below the gel point.

The slurry flocculation seen at elevated temperatures is likely related to the effect of temperature on solubility. From the data in Figure 11, the concentration of Zn and Bi ions increases by approximately an order of magnitude. The increased solubility of the powder as temperature is increased would affect the polyelectrolyte dispersant by complexation or condensation of the counterions to the adsorbed layers. This will collapse the electrolyte layers and could reduce the zeta potential to create a weakly flocculated state. These effects are in agreement with the mechanism proposed in Chapter 1, where the stability of the powder is proposed to relate to the complexation of Zn^{2+} in the dispersant layers. However, a further study of the impact of divalent cations with temperature is needed to insure that the proposed mechanism of ion complexation in the polyelectrolyte is occurring. It is possible that the dispersant solubility changes with temperature as well, or that the dissolved agarose interacts with the polyelectrolyte dispersant.

To conclude the observations, agarose will gel in the PEG400 solution, it appears to prevent some colloidal instability at elevated temperature, the gelation behavior is unaffected by addition of agarose to the CPV slurry, and the gelled values of the agarose-CPV slurry elastic modulus are sufficient to make gel cast parts. However, the flocculation of the slurry at elevated temperatures will impact the produced parts.

From Table 4, the green density given by each production method reflects the sintered density achievable in each sample. The isopressed samples were formed in order to act as a baseline for judging the colloidal processing techniques. These samples form at nearly 46.6 % theoretical density (TD) and sinter into fairly dense ceramics (92% TD). Slip casting was most effective in producing dense green bodies, but required a casting time of two weeks. Green densities are near 62 %TD, and the sintered density is

correspondingly high. The density of these samples is very near that predicted by the rheological modeling for the maximum packing fraction (see Section 1). This is attributed to the use of the plasticizing agent (PEG400) in slip casting, which inhibits the formation of cation complexes in the dispersant layers. Additionally, the ion concentration in the fluid is not expected to rise in slip casting, as the fluid phase is drawn out of the sample by capillary action. Clearly, the colloidally processed powder can achieve high density green bodies. The agarose gelcast samples were of lower density due to the necessity of achieving fluid flow prior to casting. This required a lower slurry volume fraction of 40 volume %. The samples densified to 88% TD with a large variability in density, and their electrical characteristics were poor and exhibited catastrophic shorting. The use of an isopressing step after casting using agarose gelcasting raised the sintered density of parts to 95% TD and lowered variability significantly. A green density greater than 50 % theoretical is not sufficient in itself to provide sintered bodies with reasonable electrical properties. The microstructure of the final part is also impacted by the casting method. Table 4 shows that slip casting produced parts with the smallest final pore sizes, and suggests that the microstructure of these samples is more uniform than the gelcasting method. Interestingly, even though agarose gelcasting has an average sintered pore size lower than the isopressed powder, the variation in pore size is such that lower densities are produced in the final part.

Sintering studies for ZnO varistor powders generally have focused on the mixed oxide powder route, which requires sintering temperatures of 900 to 1400 °C in air (29-32). Sintering and grain growth is largely dominated by the use of a liquid phase formed at the ZnO/ Bi_2O_3 eutectic (about 740 °C) that induces liquid sintering. For the powders used in this study, with well-distributed dopants and a surface concentration high in bismuth, densification is active at 732 °C with a hold time of 16 hours. This produces the target grain size of 0.5 micron necessary for obtaining the desired electrical properties. The sintered microstructures of these compacts shown in Figure 12 show a mean grain size of this order, and indicate that the colloidal processing operations used in this technique have not affected grain growth. This powder contains a bismuth concentration of 0.56 mole%, which is approximately twice that needed for grain boundary coverage. As a result, there are regions in the microstructures of all samples primarily composed of bismuth oxide (known as "bismuth stars", not shown). These regions do not appear to be interconnected, and they are not expected to affect the electrical properties. The higher bismuth concentration is used in these powders to achieve the increased sinterability required by the grain size restriction, and the bismuth "stars" do not inhibit the target electrical characteristics.

The electrical characterization tests between the isopressed dry powder and slip cast parts give very comparable results, as shown in Figure 13. The slip cast parts, which are slightly higher in density, require slightly higher electric fields to reach the same current density as the isopressed powder. While there are several microstructural factors that might explain the slight difference in field magnitude, one possible reason for this behavioral trend is that the higher density varistors have a slightly smaller grain size (on the order of 10%). Confirming grain size differences of 10% or less in submicrometer, complex, multicomponent oxides is beyond the scope of the present work. Encouragingly, both slip cast and isopressed, high field, chem-prep varistors had very respectable nonlinearity coefficients on the order of 30 for a current density range of 2.5

to 8.75 A/cm^2. Electric fields of approximately 42 kV/cm at 5 A/cm^2 were measured for both isopressed and slipcast varistor elements. This high switching field behavior which could lead to substantial miniaturization of varistor components for given applications, since conventional varistor materials have switching fields on the order of 1.5 kV/cm at 5 A/cm^2.

Conclusions

Of the colloidal processing methods tested for part fabrication, slip casting formed samples of highest green and fired density, least sample variability, and met the desired electrical characteristics. The aqueous processing techniques used did not cause leaching of the components or deleterious microstuctural effects in the parts. Agarose gelcasting was not successful as a production technique as a single process or by using a second isopressing step to increase density values. Dissolution of zinc and bismuth aqueous species during the heating process had deleterious effects on the colloidal stability of the particles and lead to a flocculated system. The colloidal instability of the particles prevented the use of high volume fraction slurries and the production of high density parts. The ambient temperature process of slip casting was successful in achieving near theoretical high density values in green compacts. Slipcast samples were comparable with isopressed compacts in electrical properties, but agarose cast parts exhibited catastrophic shorting even with a post isopressing step. The reason for electrical breakdown in the agarose produced samples could not be determined. The origin of electrical breakdown "flaws" is an ongoing study in our laboratories.

Section 3: Alternative Processes

Introduction

All testing to date has been performed in aqueous solvent. Processing difficulties with the powder are believed to relate to the dissolution of the dopant ions in low concentrations to cause particle flocculation. This limits the achievable powder content in the suspension, but the milling processes used have shown that very dense green samples can be formed which achieve the desired final electrical properties.

Agarose was chosen as the gelation binder due to its activity and lack of chemical reactions. The free radical initiated gelation procedure using acrylamide and methylene bis acrylamide was tested with the chemically prepared ZnO powder. The reaction could not be initiated, and it is theorized that one of the dopants is a free radical scavenger. This prevents the initiation of the polymerization reaction to form the desired gel structure. The high temperature required for agarose dissolution in water (90°C) limits the stability of the ZnO dispersion, and raises the evaporation rate of the solvent in the de-airing step. This can lead to failure of the casting process. One alternative is to find another gelation mechanism other than agarose that would be active at lower temperatures. We have investigated some small molecule hydrogelators for applicability to the near net shape process. There are a number of chemistries that claim to form gels in both aqueous and non-aqueous solvents. (33-38).

An alternative process that could overcome the difficulties seen in the aqueous solvent system would involve using a non-aqueous solvent such as an alcohol or glycol, which would not support the dissolution of dopants. Success in such a process requires the determination of an effective particle dispersant for the system, and application of the attrition milling method to reduce the agglomerate size. A gelation mechanism for the chosen solvent also needs to be identified.

The following sections are the investigations into alternative methods and a review of processes from the literature which have the potential for success in near net shape forming of the chemically processes zinc oxide material.

Small Molecule Gelators

Some recent publications present studies of the formation of small molecule (sub 400 g/mol molecular weight) which have a thermal gelation transition. We investigated a chosen material called N^{α}-Lauroyl-L-lysine methyl ester. From our investigations, it is apparent that the small molecules do show a transition in solubility in water based on heating. On cooling, we do not believe that a true gel is formed. Our definition for a "true gel" is a system in which strands have crosslinks. Our observations of the synthesized gel showed a structure that was irreversibly broken down by mechanical action. This suggests that the hydrogelators proposed in the literature are precipitated needles, which have a weak attraction to support stress. Once sheared, the needles do not restructure to form a gel. Crosslinked needles are not present. It may be possible to add a derivative molecule which acts as a crosslinking point between precipitating needles (such as the use of methylene bis acrylamide as a crosslinker in poly acrylamide gels).

We are also testing a separate molecule based on L-lysine with similar claims for gelation ability (reference M. Suzuki, et al.). Once synthesized, we will test the rheological properties of the system to determine the applicability to near net shape forming.

Lysine hydrogelator synthesis procedure:

N^{α}-Lauroyl-L-lysine methyl ester (C1AmiNH_2): A suspension of N-Lauroyl-L-lysine (0.33 mol) in methanol (800 ml) was saturated with dry HCl (gas) in an ice bath. After standing overnight at room temperature, excess HCl and methanol were completely removed by evaporation. THF (400 ml) was added to the residue, and the solution was allowed to stand in a refrigerator for 6 hours. The resulting white precipitate was filtered, washed with diethyl ether, and then dried. The HCl salt of C1AmiNH_2 was dissolved in water (2 L), and a large excess or morpholine (2.3 mol) was added with vigorous stirring. The white precipitate was collected by filtration, washed with water, and then dried. C1AmiNH_2 was purified by recrystallization from ligroin. (96%)

N^{α} -(11 Bromoundecanoyl)-N′-lauroly-L-lysine methyl ester (C1AmiC11Br): 11-Bromoundecanoyl chloride (13.0 mmol) was slowly added to a dry THF solution (100 ml) of the C1AmiNH_2 (11.6 mmol) and triethylamine (60.0 mmol) at 0°C with stirring. The resulting solution was stirred at room temperature for 24 hours. Then it was reheated to 60°C and was filtered hot; the filtrate was evaporated to dryness. The crude product was purified by two recrystallizations from ethyl acetate/diethyl ether (97%).

(2d) N^{α} -[11-(4-Phenylpyridinium)undecanoyl]-N-laurolyl-L-lysine ethyl ester bromide: A solution of C1AmiC11Br (8.3 mmol) and 4-phenyl-pyridine (150 ml) in dry DMF (20 ml) was heated at 100°C for 48 h under a nitrogen atmosphere. The resulting solution was evaporated to dryness. The product was obtained by two recrystallizations from ethyl acetate/diethyl ether (98%).

Other Procedures

Dispersions in Non-Aqueous Solvents

From the paper by Yanez et al., use of a non-aqueous solvent creates a situation where temperature can be used to control rheology and the development of a particle gel. In the system of alumina, poly(12-hydroxy stearic acid), and hexanol (a marginal solvent for the dispersant), a reduction in temperature induces the formation of a particle gel due to the loss in solubility of the dispersant. A similar system was used by Rueb and Zukowski involving silica particles coated with octadecyl in a solvent of hexadecane (39). For high enough solids loading, it may be possible to form parts in the poly (12-hydroxy stearic acid/hexanol system) and dry them.

Freeze drying may be an option. Tert-butanol is a solvent with a melting point of 26 C. Dispersion of the varistor material would allow for processing at warm

temperatures, and freeze drying at near room temperature. If the varistor material exhibits the same limitation in volume fraction as seen in the aqueous system, isopressing can be attempted to raise the green density before sintering.

Another concept involves the use of triblock co-polymers of poly (methylmethacrylate) (PMMA) and poly (tert butyl acrylate) (40). These materials have a soluble midblock in 2-hydroxy-hexanol, but the PMMA endblocks are insoluble below 70 °C. Heating the slurry and polymer above 70°C generates a fluid solution, and on cooling, the PMMA precipitates to form a gel in the suspension. The synthesis of this polymer is not trivial (41), and market sources are very expensive, suggesting that this procedure is not feasible for scale-up to production applications. However, there may be other polymers with similar structure that would behave likewise in another solvent.

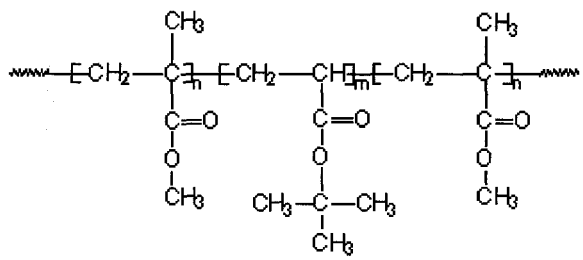

We are considering the application of PMMA spheres as a thermal binder. PMMA spheres are very low cost and readily available. We plan to test using alumina slurries to see if melting and precipitation of PMMA spheres in 2-hydroxy-hexanol will lead to a green body which can be processed into a final part. The processes should be similar to the alternative process of injection molding.

References

1. W. M. Sigmund, N.S. Bell, and L. Bergstrom, *J. Am. Ceram. Soc.* 83, 1557 (2000).
2. A. Vojta and D.R. Clarke, *J. Am. Ceram. Soc.* 80, 2086 (1997).
3. R. G. Dosch, B. A. Tuttle, and R. A. Brooks, *J. Mater. Res.* 1, 90 (1986).
4. T. J. Gardner and S. J. Lockwood, Sandia Report, SAND87-2194, Feb. 1988.
5. K. M. Kimball and D. H. Doughty, Sandia Report, SAND86-0713, Aug. 1987.
6. T. J. Gardner, D. H. Doughty, S. J. Lockwood, B. A. Tuttle, and J. A. Voigt, in *Ceramic Transactions Vol. 3, The American Ceramic Society, Inc.*, 1989.
7. L. Bergstrom, K. Shinosaki, H. Tomiyama, and N. Mitzutani, *J. Am. Ceram. Soc.* 80, 291 (1997).
8. L. Bergstrom, *J. Am. Ceram. Soc.* 79, 3033 (1996).
9. J. Cesarano, I. A. Aksay, and A. Bleier, *J. Am. Ceram. Soc.* 71, 250 (1988).
10. J. Cesarano and I. A. Aksay, *J. Am. Ceram. Soc.* 71, 1062 (1988).
11. C.F. Baes and R.E. Mesmer, The Hydrolysis of Cations, Krieger Publishing Co., Malabar, FL, 1986.
12. S.B. Johnson, A.S. Russell, and P.J. Scales, *Colloids and Surfaces* A 141, 119 (1998).
13. A.S. Dukhin and P.J. Goetz, *Adv. Colloid Interface Sci.* 92, 73 (2001).
14. A.S. Dukhin and P.J. Goetz, *Colloids and Surf. A: Physicochemical and Engineering Aspects* 192, 267 (2001).
15. A. S. Dukhin, personal communication.
16. R.D. Porasso, J.C. Benegas, and M.A.G.T. van den Hoop, *J. Phys. Chem.* B 103, 2361 (1999).
17. J. Sun, L. Bergstrom, and L. Gao, *J. Am. Ceram. Soc.* 84, 2710 (2001).
18. T. Abraham, A. Kumpulainen, Z. Xu, M. Rutland, P. M. Claesson, and J. Masliyah, *Langmuir* 17, 8321 (2001).
19. M. Zeghal and L. Auvray, *Europhysics Lett.* 45 482 (1999).
20. K. Podhajecka, M. Stepanek, K. Prochazka, and W. Brown, *Langmuir* 17, 4245 (2001).
21. H. H. Rmaile and J. B. Schlenoff, *Langmuir,* 18, 8263 (2002).
22. R.R. Netz, *J. Phys.: Condens. Matter* 15, S239 (2003).
23. J. H. D. Hampton, S.B. Savage, and R. A. L. Drew, *J. Am. Ceram. Soc.* 71, 1040 (1988).
24. Wasche, G. Steinborn, and T. Rabe, *Ceramic Forum International* 72, 24 (1995).
25. A.J. Fanelli, R.D. Silvers, U.S. Patent Number 4,734,237, 1988.
26. A.J. Fanelli, R.D. Silvers, W.S. Frei, J.V. Burlew, and G.B. Marsh, *J. Am. Ceram. Soc.* 72, 1833 (1989).
27. J. Cesarano, III, Ph. D. Dissertation, University of Washington, Seattle, WA, 1989.
28. K. C. Labropoulos, S. Rangarajan, D.E. Niesz, and S.C. Danforth, *J. Am. Ceram. Soc.* 84, 1217 (2001).
29. D. Dey and R.C. Bradt, *J. Am. Ceram. Soc.* 75, 2529 (1992).
30. T. Senda and R. C. Bradt, *J. Am. Ceram. Soc.* 73, 106 (1990).
31. C.-H. Lu, N. Chyi, H.-W. Wong, and W.-J. Hwang, *Mat. Chem. Phys.* 62, 164 (2000).
32. J. Kim, T. Kimura, and T. Yamaguchi, *J. Am. Ceram. Soc.* 72, 1541 (1989).

33. G. Wang and A.D. Hamilton, "Low Molecular Weight Organogelators for Water," *Chem. Comm.* (2003) 310-311.
34. M. Suzuki, M. Yumoto, M. Kimura, H. Shirai, and K. Hanabusa, "A Family of Low-Molecular-Weight Hydrogelators Based on L-Lysine Derivatives with a Positively Charged Terminal Group," *Chem. Eur. J.* 9(2003) 348-354.
35. R.J.H. Hafkamp, M.C. Feiters, and R.J.M. Nolte, "Organogels from Carbohydrate Amphiphiles," *J. Org. Chem.* 64 (1999) 412-426.
36. F.S. Schoonbeek, J.H. van Esch, R. Hulst, R.M. Kellogg, and B.L. Feringa, "Geminal Bis-ureas as Gelators for Organic Solvents: Gelation Properties and Structural Studies in Solution and in the Gel State," *Chem. Eur. J.* 6 (2000) 2633-2643.
37. J. van Esch, F. Schoonbeek, M. de Loos, H. Kooijman, A.L. Spek, R.M. Kellogg, and B.L. Feringa, "Cyclic Bis-Urea Compounds as Gelators for Organic Solvents," *Chem. Eur. J.* 5 (1999) 937-950.
38. S. van der Laan, B.L. Feringa, R.M. Kellogg, and J. van Esch, "Remarkable Polymorphorism in Gels of New Azobenzene Bis-urea Gelators," *Langmuir* 18 (2002) 7136-7140.
39. C. Rueb and C.F. Zukoski, *J. Rheol.* 41 (1997) 197.
40. J.K. Montgomery, Peter, L. Drzal, K.R. Shull, and K.T. Faber, "Thermoreversible Gelcasting: A Novel Ceramic Processing Technique," *J. Am. Ceram. Soc.* 85 [5] (2002) 1164-68.
41. S.K. Varshney, C. Jacobs, J.-P. Hautekeer, P. Bayard, R. Jerome, R. Fayt, and P. Teyssie, "Anionic Polymerization of Acrylic Monomers. 6. Synthesis, Characterization, and Modification of Poly(methyl methacrylate)-Poly(tert-butyl acrylate) Di- and Triblock Copolymers," *Macromolecules* 24 (1991) 4997-5000.

Distribution:

1	MS0885	G.E. Pike, 1801
1	MS0888	R. A. Anderson, 1843
1	MS0889	S. J. Glass, 1843
1	0889	C. S. Watson, 1843
1	MS1349	K. G. Ewsuk, 1843
1	1349	W. F. Hammetter, 1843
1	MS1411	B. A. Tuttle, 1843
1	MS1411	J. Liu, 1846
2	1411	N. S. Bell, 1846
4	1411	J. A. Voigt, 1846
1	MS0515	S. G. Barnhart, 2561
1	0515	J. D. Keck, 2561
1	MS0521	R. A. Pike, 2561
1	MS0959	T. J. Gardner, 14154
1	0959	G. R. Burns, 14154
1	0959	C. B. DiAntonio, 14154
1	0959	J. T. Gibson, 14154
1	0959	J. P. Hanlon, 14154
3	0959	S. J. Lockwood, 14154
1	0959	P. Yang, 14154
1	MS9018	Central Technical Files, 8945-1
2	0899	Technical Library, 9616
1	0612	Review & Approval Desk, 9612 For DOE/OSTI